AIMS Mathematics, 11(1): 1878–1899.
DOI: 10.3934/math.2026078
Received: 21 October 2025
Revised: 02 December 2025
Accepted: 15 December 2025
Published: 20 January 2026

https://www.aimspress.com/journal/Math

Research article

Non-linear transformations combinations on fractal structures and aggregates

Sancho Salcedo-Sanz[1,*], Pablo Álvarez-Couso[2], Luis Castelo-Sardina[2] and Jorge Pérez-Aracil[1]

[1] Department of Signal Processing and Communications, Universidad de Alcalá, 20805 Alcalá de Henares, Madrid, Spain

[2] Department of Design and Image, Universidad Complutense de Madrid, 28040, Madrid, Spain

* **Correspondence:** Email: sancho.salcedo@uah.es.

Abstract: This paper discusses the effects of applying different non-linear transformations in combination to well-known fractal structures and aggregates, to obtain novel fractal images. Five different non-linear transformations are selected to be combined, and applied to existing aggregates, and the new fractal structures obtained are discussed. We show how different non-linear transformations effects (bending effects, diffusion effects, etc.) can be combined just by function composition processes, and their final results as new fractal images. We analyze the effects of the combination of non-linear transformations over classical fractals such as the Sierpinski triangle and Sierpinski carpet, in terms of the fractal dimension of the new structures created. Finally, we will also show the effect of the non-linear transformation on other fractal structures, such as diffusion limited aggregation and strange attractors.

Keywords: fractal images generation; non-linear transformations; transformations combination; fractal structures; fractal aggregates
Mathematics Subject Classification: 28A80, 46Txx

1. Introduction

The creation of new aesthetic fractal images from fractal aggregate generation methods has called the attention of researchers and artists from the 80's [1, 2]. For instance, non-equilibrium growth models such as diffusion limited aggregation (DLA) [3, 4] were proposed in the 80's as a way of generating self-organized fractal-like particle clusters [5]. Iterated function systems (IFS) [6–8] have also been proposed for fractal image generation, and they have been widely used in fractal art and computer graphics [9–12]. Strange attractors (SA), are the solutions of non-linear iterative equations, and they have been studied in statistical physics [13,14] and also used for generating fractal images and

aggregates [15]. Lindenmayer systems (L-systems) [16], is another family of methods for generating fractal structures, which have been applied to construct fractal images, in many cases related to plants and vegetation representation [17, 18]. There are other works in the literature that have described hybrid approaches, merging some of these classical fractal aggregates generation methods (and also other alternatives), to obtain new fractal structures [19–23].

In previous years, different works have studied the effect of non-linear transformation for generating new fractal images [24]. In [25], non-linear IFS were described to generate fractal patterns over regular polygons. In other cases, shape inversion transformations have been applied. For instance, in [26] the star-shaped set inversion was studied for fractal image generation. In [27], the idea of star-shaped set inversion fractals was generalized, using iterations from fixed point theory. New aesthetic fractal computer graphics were obtained in this case. In [28] shape inversions were applied to Mandelbrot-like fractals in the complex plane. In [29], the p-circle transformation was studied, and novel fractal structures were obtained by the application of this transformation. In [30], different families of fractal tilings were described and applied to obtain *Escher-like* fractal images, which were further processed by applying non-linear transformations, such as stereographic projection, in order to obtain spherical representation of the fractals.

As shown above, the application of non-linear transformations to existing fractal structures has been considered an efficient method to obtain novel fractal images with different properties. In this paper, we analyze how non-linear transformations can be combined (sequentially applied by function composition) to fractal structures and aggregates in a simple way, to obtain new fractal structures, in many cases with marked aesthetic properties. Fractal structures such as the Sierpinski triangle, the Sierpinski carpet, and aggregates from DLA, SAs, L-Systems, and IFS are considered as initial shapes, which will be transformed by applying combinations of five different non-linear transformations. The composition of the different non-linear transformations to the initial fractal images and aggregates leads to different final fractal structures, including effects such as bending forms, or diffusion effects on aggregates. We will characterize the new fractal structures by means of their fractal dimensions

The remainder of the paper has been structured in the following way: Section 2 describes some classical fractal image generation methods such as DLA, IFS, L-Systems and SA construction. We also describe different non-linear transformations whose effects on fractal aggregates will be evaluated, as well as the box-counting method for the fractal dimension calculation for the newly generated fractals. Section 3 presents the results obtained and discusses the effect of applying combinations of different non-linear transformations to well known fractal structures and aggregates. Finally, Section 4 closes the paper by extracting some conclusions and remarks on the research.

2. Methods

This section summarizes some classical methods used to generate fractal 2D aggregates (fractal-like particle clusters in a 2D plane). We specifically focus on diffusion limited aggregation and strange attractors fractals.

2.1. Fractal structures and aggregates

2.1.1. Diffusion limited aggregation

Diffusion limited aggregation (DLA) [3, 31] is a simple algorithm that generates random fractal clusters or aggregates [32]. Aiming at illustrating the DLA method, we have considered the general DLA model implementation described in [33]. This DLA model takes into account a unique seed at the beginning of the simulations, located at the center of a given discrete lattice, which will be the initial cluster to be grown. Then, *particles* are sequentially released at a circle distant from the cluster. The positions of these particles are modified by means of a random walk. The distance between the center of the lattice and the launching circle is denoted as R_l. The random walks are defined as follows:

$$\begin{pmatrix} x_{n+1} \\ y_{n+1} \end{pmatrix} = \begin{pmatrix} x_n \\ y_n \end{pmatrix} + \begin{pmatrix} \cos(\varphi + \lambda\theta_n) \\ \sin(\varphi + \lambda\theta_n) \end{pmatrix}, \tag{2.1}$$

where x_n and y_n are the particle positions at the nth step of the random walk, $\varphi \in [-\pi, \pi]$ is a random angle that defines the direction of the particle's trajectory, $\lambda \in [0, 1]$ is a parameter that introduces the random component of the trajectories, and $\theta_n \in [-\pi, \pi]$ is a random direction. The random walk also ends if the distance between the particle and the cluster is larger than a killing radius R_k. In the latter case, the particle is eliminated and a new one is released at the launching circle R_l. Usually, the relationship between R_l and R_k is defined as:

$$R_l = R_{max} + R_0, \tag{2.2}$$

where R_{max} is the maximum distance from the center of the lattice to a particle belonging to the cluster, and R_0 is a defined radius. The killing radius R_k is then defined as:

$$R_k = 2R_{max} + R_0 = R_{max} + R_l, \tag{2.3}$$

which gives the relationship between R_l and R_k. Figure 1 shows the DLA procedure, and Figure 2 shows an example of a fractal structure generated by DLA simulation.

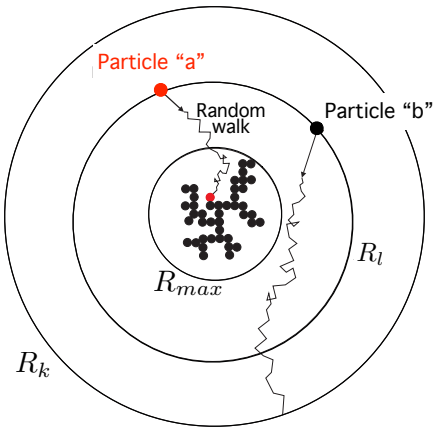

Figure 1. Example of a DLA simulation construction.

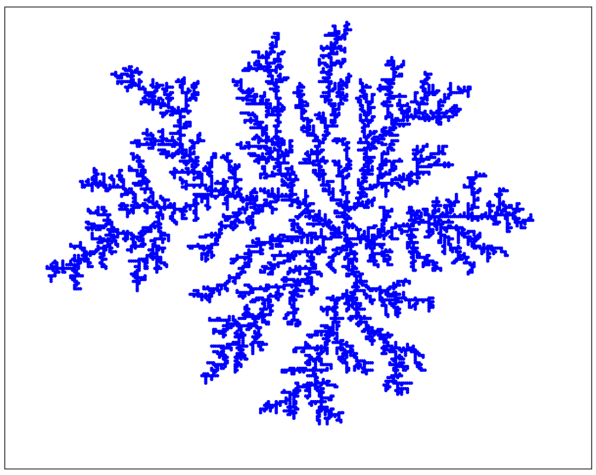

Figure 2. Example of a fractal structure in the phase space (x vs. y), obtained by means of a classical DLA simulation (around 8000 particles).

2.1.2. Strange attractors

Another method to obtain fractal-like 2D structures is to consider strange attractors (SA) of dynamical systems with chaotic behavior [13, 14, 34]. A SA can be seen as the solution to a non-linear dynamic system (usually chaotic), in such a way that the pattern generated in the phase space is fractal in nature. Usually, SAs are generated using iterated non-linear maps, which can be quadratic, cubic, etc. For instance, the general two-dimensional iterated quadratic map can be described as follows:

$$\begin{cases} x_{n+1} = a_1 + a_2 x_n + a_3 x_n^2 + a_4 x_n y_n + a_5 y_n + a_6 y_n^2 \\ y_{n+1} = a_7 + a_8 x_n + a_9 x_n^2 + a_{10} x_n y_n + a_{11} y_n + a_{12} y_n^2. \end{cases} \tag{2.4}$$

Note that, as reported in [15], a small percentage of the solutions from Eq (2.4) are SAs (depending on the parameters $\{a_1, \ldots, a_{12}\}$) and, in fact, some of them are chaotic, but there are others intermittent or convergent to a periodic orbit. Figure 3 shows some examples of SAs, obtained from Eq (2.4), initialized with $(x_0, y_0) = (0.6, 0.9)$.

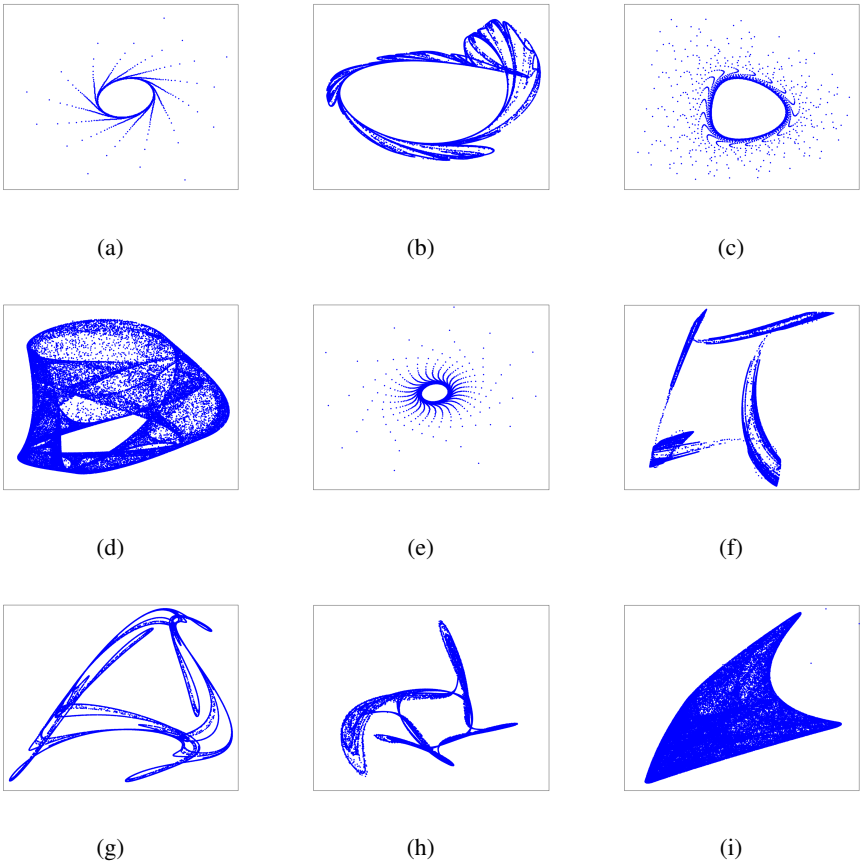

Figure 3. Examples of SAs in the phase space (x vs. y), from Eq (2.4).

2.1.3. Iterated function systems

An iterated function system (IFS) [7, 35, 36] is a way of generating fractal-like 2D aggregates and geometric patterns based on the iteration of one or more *affine transformations*, i.e., recursive transformations involving rotations, scalings, and translations [37]. They have the following general form in $\mathbb{R}^2$:

$$\begin{pmatrix} x_{n+1} \\ y_{n+1} \end{pmatrix} = \begin{pmatrix} a & b \\ c & d \end{pmatrix} \cdot \begin{pmatrix} x_n \\ y_n \end{pmatrix} + \begin{pmatrix} e \\ f \end{pmatrix}. \tag{2.5}$$

The idea behind IFS is to apply different affine transformations, in some cases with a given probability, until obtaining the desired fractal form. We illustrate the application of an IFS to obtain fractal structures in Figure 4, where we show the Sierpinski carpet aggregate. The IFS equations to generate this fractal are detailed in the Appendix section of the paper (see Appendix).

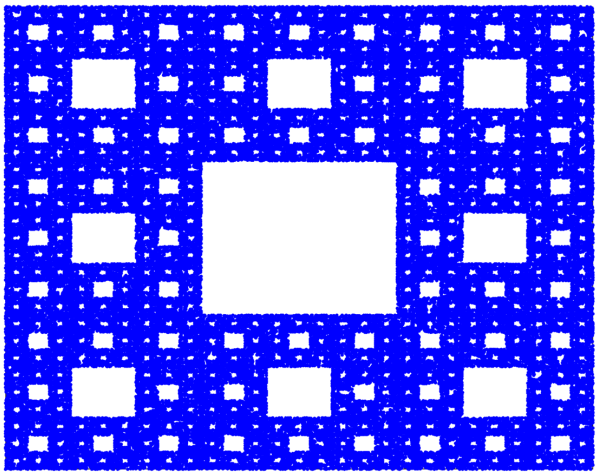

Figure 4. Example of an IFS construction of the Sierpinski carpet.

2.1.4. Lindenmayer systems (L-systems)

A Lindenmayer system or L-system [16, 38] is a well-known method to obtain fractal images [39], which, in principle, is not focused on aggregates or clusters, but it can be adapted to generate fractal-like cluster structures. A L-system can be seen as an encoder-decoder system, in which the encoding of the message is carried out through the application of certain rules involving different variables and constants, from an initial seed point. The message produced by the encoder is a sequence of symbols that will be interpreted by the decoder part of the system. The recursive application of the encoder to previous messages will generate other messages of a larger length, which will be passed to the decoder in order to obtain the fractal structure. We will illustrate the L-systems procedure in the generation of the well-known Sierpinski triangle. The L-system to generate this fractal form is the following:

Encoder: Variables : A, B
Constants : $+, -$
Seed point: A
Rule 1: $(A \rightarrow +B - A - B+)$
Rule 2: $(B \rightarrow -A + B + A-)$

Decoder: A: draw forward.
B: draw forward.
$+$: turn left 60 degrees.
$-$: turn right 60 degrees.

The iterative application of this L-system produces the Sierpinski triangle, as illustrated in Figure 5, which shows the procedure and the final fractal obtained.

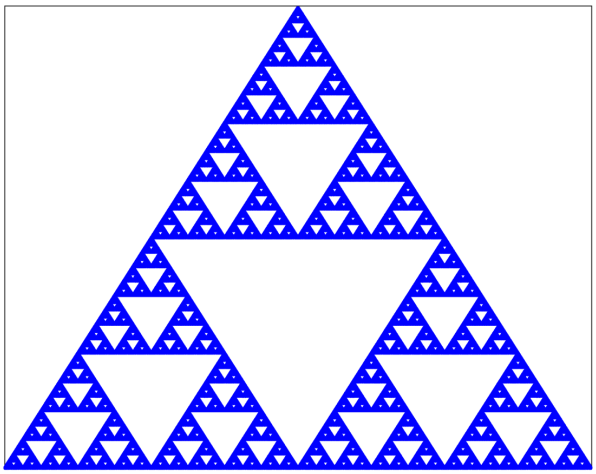

Figure 5. Sierpinski triangle construction from an L-system in the phase space (x vs. y) with $n = 9$ iterations.

2.2. Non-linear transformations in 2D spaces

Non-linear transformations in the plane can be applied to aggregates to obtain new fractal-like forms. In this paper we consider a number of well-known non-linear transformations which will be analyzed in terms of their effect on aggregates as function composites. Specifically we consider the following non-linear transformations: p-circle inversion, $z \to z^2$ transform and some variations and 2D sine transform.

The p-circle inversion [29] has been previously applied to obtain new fractals from existing structures, such as the Sierpinski triangle. Mathematical details and theorems related to this non-linear transformation can be found in [29]. In this paper, we use the p-circle inversion jointly with other non-linear transformations and apply it to obtain new fractal aggregates. The p-circle inversion can be applied in the following way:

Let us consider a p-circle C_p, characterized by a center $Q = (a, b)$, and a radius r. Then, the p-circle inversion of a point $P = (x, y)$ from C_p, is the following:

$$P_1 = \left(a + \frac{r^2(x-a)}{(|x-a|^p + |y-b|^p)^{(2/p)}}, b + \frac{r^2(y-b)}{(|x-a|^p + |y-b|^p)^{(2/p)}}\right). \tag{2.6}$$

We will denote the p-circle inversion as f_1 in this paper, so $f_1(P) = P_1$.

The second non-linear transformation considered in this work is obtained from the non-linear transformation in the complex plane, which produces $z \to z^2$. Specifically, this transformation has the following effect when applied at a point $P = (x, y)$:

$$P_2 = \left(x^2 - y^2, 2xy\right). \tag{2.7}$$

We will denote this transformation as f_2, so $f_2(P) = P_2$. We also consider two other non-linear transformations based on f_2, as follows:

$$P_3 = \left(x^2 - y^2, x^2\right) \tag{2.8}$$

and

$$P_4 = \left(x^2 - y^2, y^2\right). \tag{2.9}$$

We will denote these transformations as f_3 and f_4, respectively, in such a way that $f_3(P) = P_3$ and $f_4(P) = P_4$. Finally, we also consider a final transformation (f_5) defined in such a way that if $P = (x, y)$, $f_5(P) = P_5$, where P_5 is defined as follows:

$$P_5 = (x + \alpha \cdot sin(y), y + \alpha \cdot sin(x)), \tag{2.10}$$

where α is a real positive parameter of the transformation.

2.3. Fractal dimension calculation

We can characterize the fractals obtained with the non-linear transformations applied, by obtaining the fractal dimensions of the new fractals. For this, we have calculated the fractal dimensions using the well-known box-counting method [40–43]. Let C be a fractal structure in 2D. The box counting method is a procedure to obtain the fractal dimension of C. To calculate this dimension for a fractal C, the box-counting algorithm works by counting how many boxes are required to cover the set. The box-counting dimension is obtained by calculating how this number changes as we make the grid finer. Let us suppose that $n(r)$ is the number of boxes of size r required to cover the set. Then the box-counting dimension is defined as:

$$\alpha = \lim_{r \to 0} \frac{log(n(r))}{log(r)}. \tag{2.11}$$

In other words, if C is a fractal set, with the fractal dimension $\alpha < 2$, then $n(r)$ scales as $r^{-\alpha}$. Note that α is also known as Minkowski-Bouligand dimension, Kolmogorov dimension, or box-counting dimension.

In this paper, we have used the implementation of the box-counting method provided by Matlab®. It operates by counting the number n of 2-dimensional boxes of size r needed to cover the nonzero elements of C, uploaded as a binary matrix. The box sizes are, in this case, considered as powers of two, i.e., $r = 1, 2, 4, \ldots, 2^P$, where P is the smallest integer such that

$$\max(size(C)) \leq 2^P. \tag{2.12}$$

If the size of C over each dimension is smaller than 2^P, C is padded with zeros to size 2^P over each dimension (for instance a 400×200 image is padded to 512×512). The output vectors $n(r)$ and r are of size $P + 1$. Equation (2.11) is then considered to obtain the fractal dimension α, as the slope of the log-log plot r vs. $n(r)$.

3. Results: construction of new fractal structures and aggregates with non-linear transformations combinations

In this section, we show the results obtained by applying the combinations of different non-linear transformations to existing (known) fractals and aggregates. We have structured this section in two

different parts: first, we will show the effect of the combination of non-linear transformations on well-known fractal structures, such as the Sierpinski carpet (Figure 4) and the Sierpinski triangle (Figure 5), shown before. We will carry out here an analysis of the fractals obtained by the non-linear transformations by calculating their fractal dimensions using the box-counting method described above. Then, we will show the effect of the non-linear transformations combination on different aggregates from DLAs and strange attractors (shown in Figure 3).

3.1. New fractals from the Sierpinski triangle and Sierpinski carpet with non-linear transformation combinations

Let us denote the Sierpinski triangle as $\mathcal{T}$, and the Sierpinski carpet as C. First, note that the effect of the f_1 non-linear transformation (p-circle) on the Sierpinski triangle ($f_1(\mathcal{T})$) and the outcome fractals obtained have been previously discussed in [29]. We reproduce the results in Figure 6(a),(b). The application of the non-linear transformation f_1 on the Sierpinski Carpet ($f_1(C)$) is shown in Figure 6(c),(d).

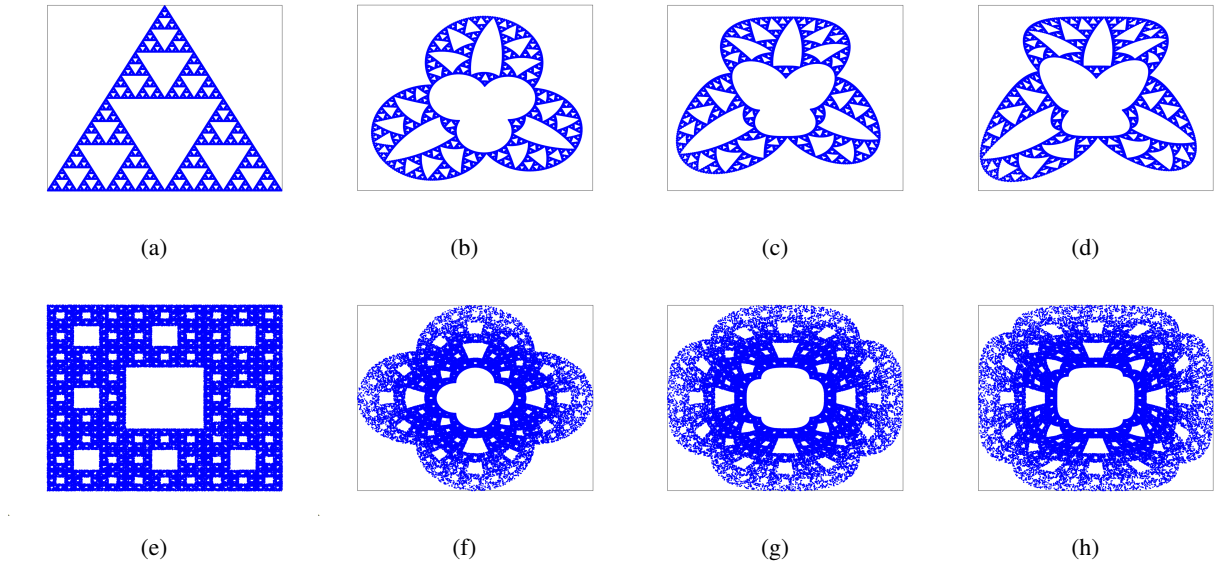

Figure 6. Application of f_1 transformation to the Sierpinski triangle, and the Sierpinski carpet, with different values of p; (a) Original Sierpinski triangle ($\mathcal{T}$); (b) $f_1(\mathcal{T})$ with $p = 2$; (c) $f_1(\mathcal{T})$ with $p = 3$; (d) $f_1(\mathcal{T})$ with $p = 4$; (e) Original Sierpinski carpet (C); (f) $f_1(C)$ with $p = 2$; (g) $f_1(C)$ with $p = 3$; (h) $f_1(C)$ with $p = 4$.

Note that the p-circle transformation can be applied with $p = 2, 3, 4$, etc. Figure 6 shows non-linear transformations of $\mathcal{T}$ and C with different values of the parameter p. These fractals can be characterized by calculating their fractal dimensions, using the box counting method described above. Figure 7 shows the log-log plot r vs. $n(r)$ graphs for the Sierpinski triangle and Sierpinski carpet fractals, as well as the application of f_1 to these fractals. Table 1 shows the fractal dimensions calculated from the log-log plots of Figure 7.

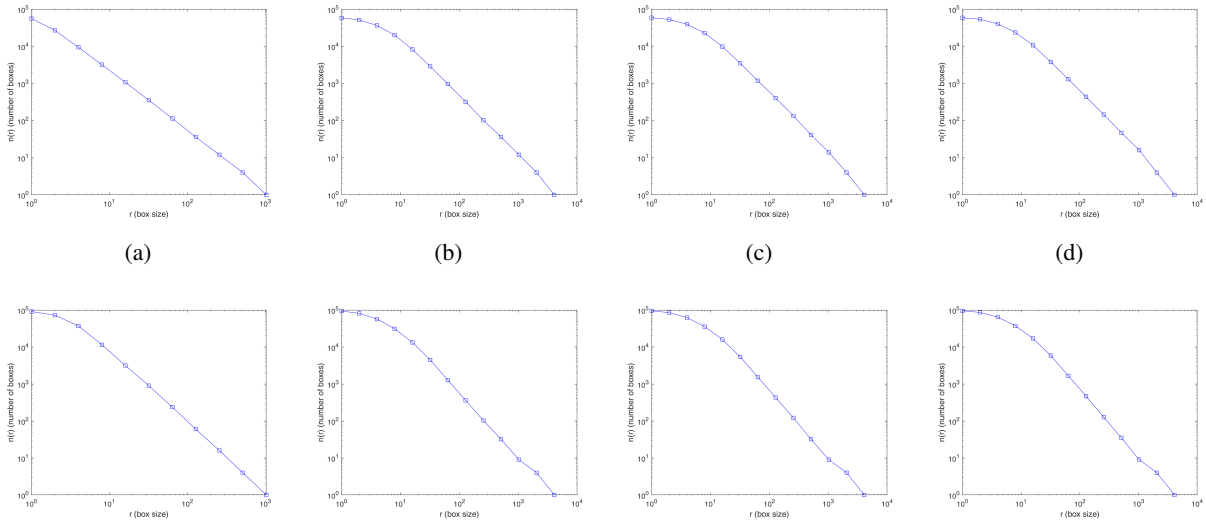

Figure 7. Evaluation of the fractal dimension calculation for the Sierpinski triangle ($\mathcal{T}$) and $f_1(\mathcal{T})$ with different values of parameter p (see Eq (2.6)), using the box-counting algorithm; (a) log-log plot r vs. $n(r)$ for the original Sierpinski triangle; (b) log-log plot r vs. $n(r)$ for $f_1(\mathcal{T})$ with $p = 2$; (c) log-log plot r vs. $n(r)$ for $f_1(\mathcal{T})$ with $p = 3$; (d) log-log plot r vs. $n(r)$ for $f_1(\mathcal{T})$ with $p = 4$; (e) log-log plot r vs. $n(r)$ for the original Sierpinski carpet; (f) log-log plot r vs. $n(r)$ for $f_1(C)$ with $p = 2$; (g) log-log plot r vs. $n(r)$ for $f_1(C)$ with $p = 3$; (h) log-log plot r vs. $n(r)$ for $f_1(C)$ with $p = 4$.

Table 1. Fractal dimensions of the Sierpinski triangle and Sierpinski carpet (original and after the application of f_1), obtained from subfigures shown in Figure 7.

Fractal	known value	Fractal Dimension (Box Counting)
Sierpinski Triangle $\mathcal{T}$	1.585	1.59
$f_1(\mathcal{T})$ $(p = 2)$	-	1.58
$f_1(\mathcal{T})$ $(p = 3)$	-	1.57
$f_1(\mathcal{T})$ $(p = 4)$	-	1.59
Sierpinski Carpet C	1.892	1.90
$f_1(C)$ $(p = 2)$	-	1.81
$f_1(C)$ $(p = 3)$	-	1.80
$f_1(C)$ $(p = 4)$	-	1.85

We now produce new fractal aggregates by composing some of the different non-linear transformations considered. For instance, Figure 8 shows the combination of different transformations applied to the Sierpinski triangle and Sierpinski carpet. Specifically, the figure shows the outcomes of the transformations $f_2(\mathcal{T})$ (a), $f_2(C)$ (d), $f_1(f_2(\mathcal{T}))$ (b), and $f_1(f_2(C))$ (e). As can be seen, the

combination of non-linear functions leads to completely different fractal forms from the original $\mathcal{T}$ and C fractals. Figure 8(c),(f) shows the log-log plots r vs. $n(r)$ for the fractals $f_1(f_2(\mathcal{T}))$ and $f_1(f_2(C))$, obtaining a fractal dimension of 1.56 and 1.8, respectively.

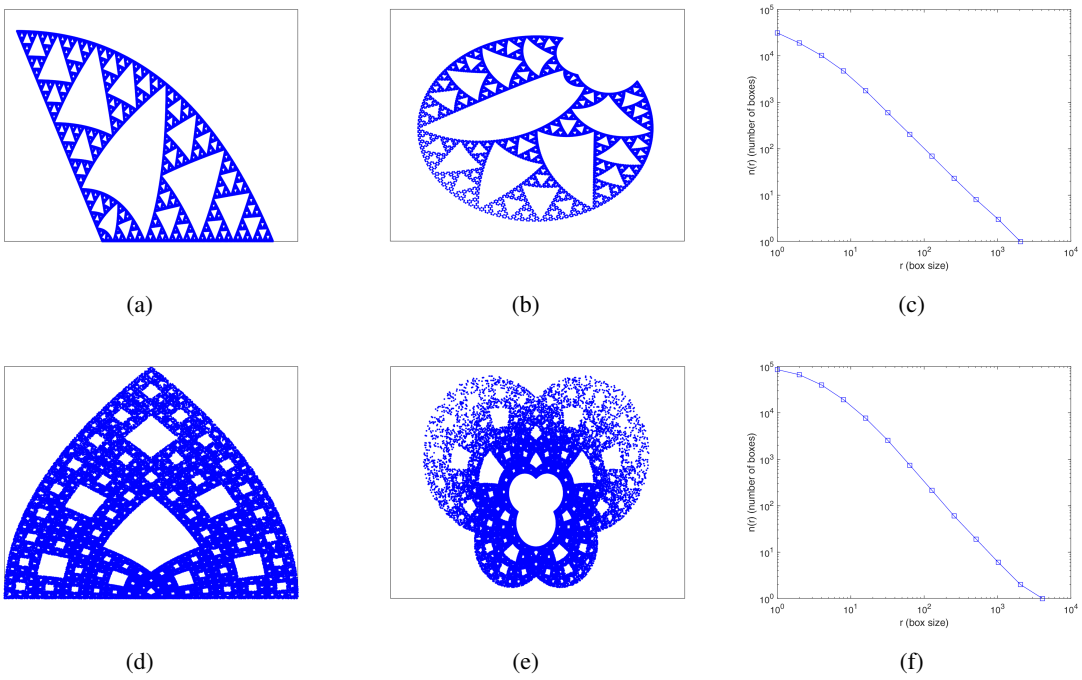

(a) (b) (c)

(d) (e) (f)

Figure 8. Application of f_2 transformation to the Sierpinski triangle and Sierpinski carpet ((a) and (c)), and the composition $f_1(f_2(\mathcal{T}))$ and $f_1(f_2(C))$, (b) and (e), respectively. We also show here the log-log r vs. $n(r)$ plots for the composition fractals ((c) and (f)).

The application of non-linear transformations f_3 and f_4 and their composition with f_1 also produces novel fractals. Figure 9 shows the application of non-linear functions $f_3(\mathcal{T})$ and $f_4(C)$ (Subfigures (a) and (d)) and the compositions $f_1(f_3(\mathcal{T}))$ and $f_1(f_4(C))$, in Figure 9(b),(e), respectively. Figure 9(c),(f) shows the log-log r vs. $n(r)$ plots for the fractals in Figure 9(b),(d), with fractal dimensions of 1.54 and 1.79 for the $f_1(f_3(\mathcal{T}))$ and $f_1(f_4(C))$ fractals, respectively.

We finally show the effect of the non-linear transformation f_5, which is very different to that of the other transformations analyzed. The sine functions involved in f_5 make a kind of "diffusion" effect when applied with different values of α (10, 20 and 50). This is illustrated for the Sierpinski triangle and carpet in Figure 10. It is easy to see the diffusion effect in both fractals when f_5 is applied. The combinations $f_1(f_5(\mathcal{T}))$ and $f_1(f_5(C))$ are also shown in Figure 11. In this combination case, the diffusion aspect of the final fractals is also evident, resulting in a kind of fractal diffusion or deconstruction from the original aggregate.

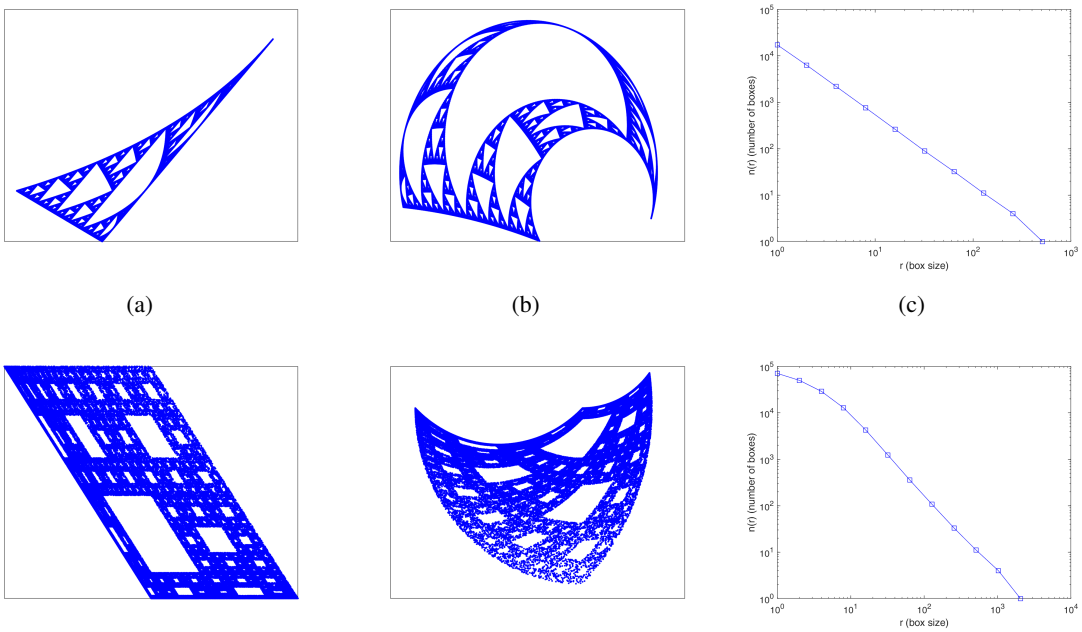

Figure 9. Application of f_3 and f_4 transformations to the Sierpinski triangle and Sierpinski carpet ((a) and (d)), and the composition $f_1(f_3(\mathcal{T}))$ and $f_1(f_4(C))$, (b) and (e), respectively. We also show here the log-log r vs. $n(r)$ plots for the composition fractals ((c) and (f)).

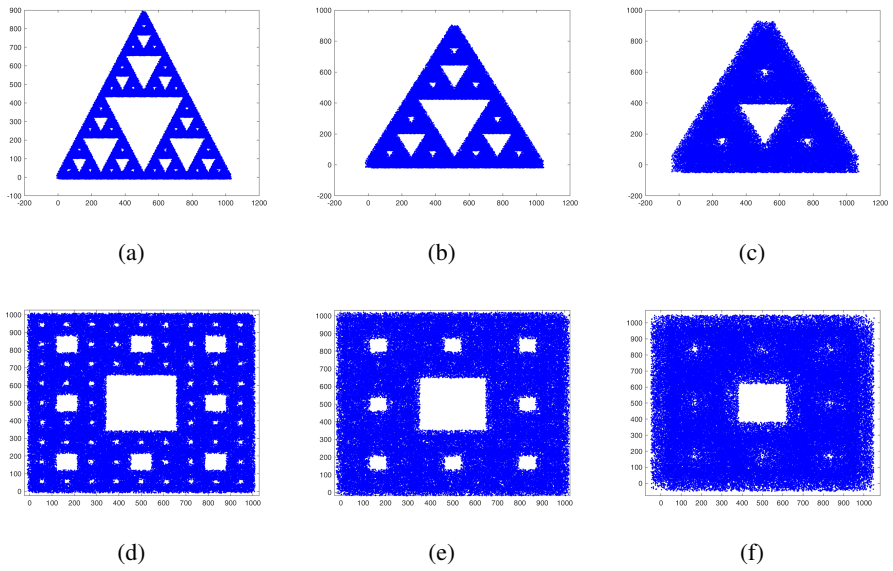

Figure 10. Effect of the f_5 application to the Sierpinski triangle ($f_5(\mathcal{T})$) and the Sierpinski carpet ($f_5(C)$), with different values of the parameter α; (a) $f_5(\mathcal{T})$ with $\alpha = 10$; (b) $f_5(\mathcal{T})$ with $\alpha = 20$; (c) $f_5(\mathcal{T})$ with $\alpha = 50$; (d) $f_5(C)$ with $\alpha = 10$; (e) $f_5(C)$ with $\alpha = 20$; (f) $f_5(C)$ with $\alpha = 50$.

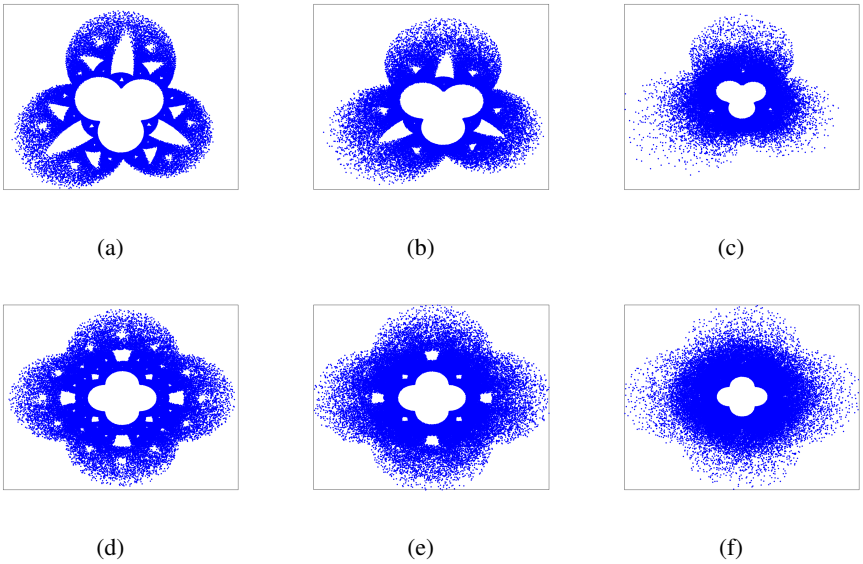

Figure 11. Effect of the composition $f_1(f_5(\cdot))$ in the Sierpinski triangle ($f_1(f_5(\mathcal{T}))$) and the Sierpinski carpet ($f_1(f_5(C))$), with different values of the parameter α; (a) $f_1(f_5(\mathcal{T}))$ with $\alpha = 10$; (b) $f_1(f_5(\mathcal{T}))$ with $\alpha = 20$; (c) $f_1(f_5(\mathcal{T}))$ with $\alpha = 50$; (d) $f_1(f_5(C))$ with $\alpha = 10$; (e) $f_1(f_5(C))$ with $\alpha = 20$; (f) $f_1(f_5(C))$ with $\alpha = 50$.

3.2. New fractal aggregates from DLA and strange attractors

Finally, we evaluate the combined application of some of the non-linear transformations considered to DLA aggregates (Figure 2) and distinct strange attractors (shown in Figure 3). The results are new fractal aggregates, different from the original ones, some of them with highly aesthetic properties. We start with the effect of the combined non-linear transformations on the DLA aggregate from Figure 2 ($\mathcal{D}$ hereafter). Specifically, we evaluate the effect of the combination f_1 and f_2. Figure 12 shows the results obtained with a color applied post-processing (the darker the blue, the earlier the particle was attached to the aggregate). Note that the non-linear transformations applied do not change the colours of the particles in the transformed aggregate, so we can approximately track the final location of the particles with different colours after the transformations. Figure 12(a) shows the original aggregate, Figure 12(b) shows the outcome of $f_1(\mathcal{D})$, Figure 12(c) shows the outcome of $f_2(\mathcal{D})$, and finally, Figure 12(d) shows the outcome of the transformation combination $f_1(f_2(\mathcal{D}))$. As can be seen, the non-linear transformations applied on their own to DLA aggregates do not have a deep effect on this aggregate, which still keeps the classical (recognizable) form of a DLA structure. This is somehow expected, given the usual circular symmetry of DLA aggregates, which makes the p-circle transformation (f_1) produce much less effect in these kind of structures. Note that this causes the combination of non-linear transformations not to have a very different effect in this fractal compared to the application of $f_2(\cdot)$ on its own to the original aggregate.

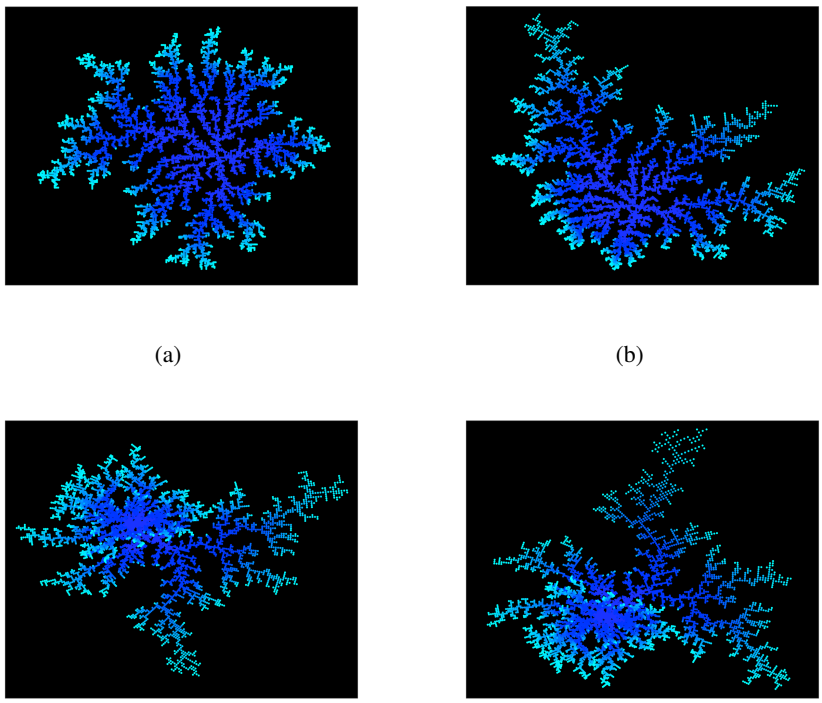

Figure 12. Application of f_1 and f_2 transformations to the DLA aggregate ($\mathcal{D}$); (a) Original aggregate ($\mathcal{D}$); (b) Non-linear transformation $f_1(\mathcal{D})$; (c) Non-linear transformation $f_2(\mathcal{D})$; (d) Non-linear transformation $f_1(f_2(\mathcal{D}))$.

The application of the combination of different non-linear transformations to SA aggregates is now described. Figure 13 shows the application of non-linear transformation $f_1(\cdot)$ to the SAs in Figure 3. In turn, Figure 14 shows the application of the combination $f_1(f_2(\cdot))$ to the SAs in Figure 3. As can be seen in these figures, the effect of the non-linear transformations combinations on SAs depends much on the original aggregate. The differences obtained after the composition of non-linear transformations are evident in the figures: In some cases the effect of $f_1(f_2(\cdot))$ is quite similar to that of $f_2(\cdot)$ on its own, such as in Figure 3(a), (c) and (e) SAs. However, in other aggregates the differences are much stronger, such as in Figure 3(b), (d) or (f). In the majority of cases, the final results of the application of non-linear transformations are highly aesthetic fractal aggregates, which can be further highlighted by a post-processing. Figure 16 shows a particular example of the application of non-linear transformations and their combination to SAs with coloring post-processing (again, the darker the blue, the earlier the particle was added to the aggregate). As can be seen, the application of non-linear transformations results in attractive artwork fractal patterns based on SAs. Figure 15 shows the recursive combination of non-linear transformations f_1 and f_2 to a different SA, with colouring post-processing, to obtain different aesthetic fractal aggregates from the initial SA.

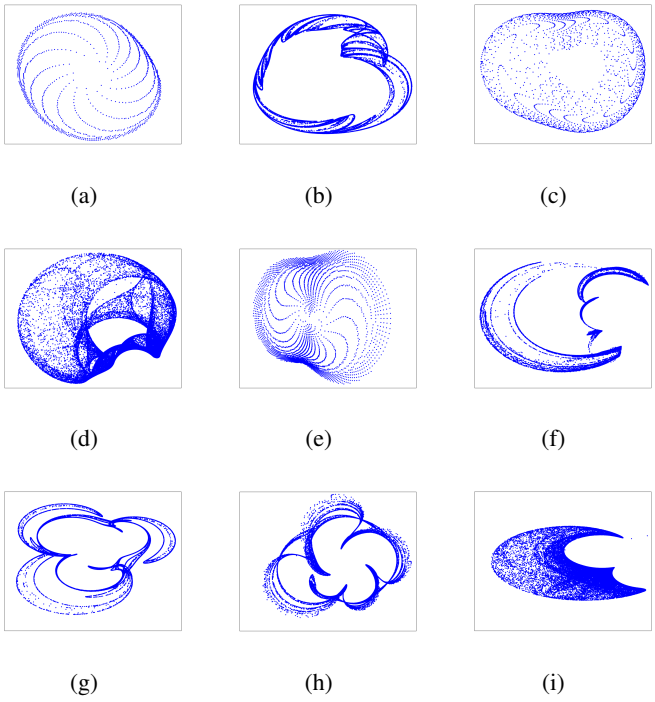

Figure 13. Application of non-linear function f_1 to the SAs in Figure 3.

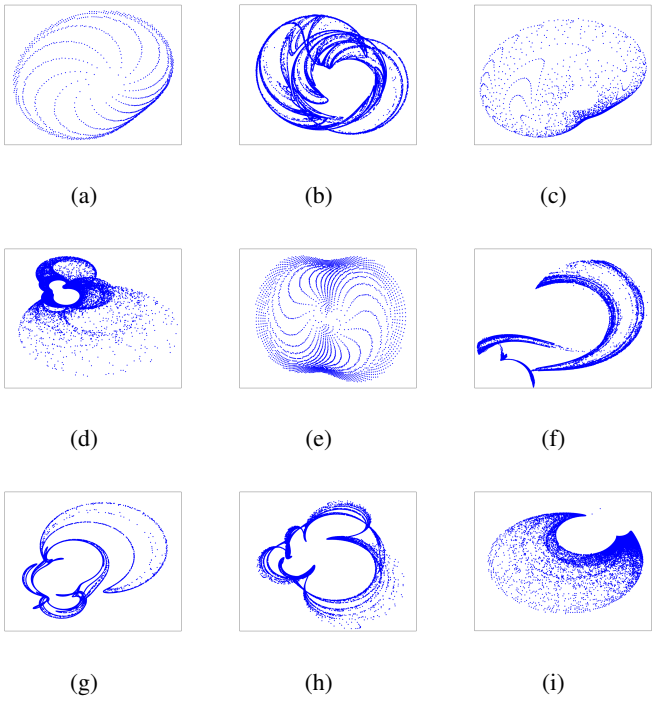

Figure 14. Application of composition $f_1(f_2(\cdot))$ to the SAs in Figure 3.

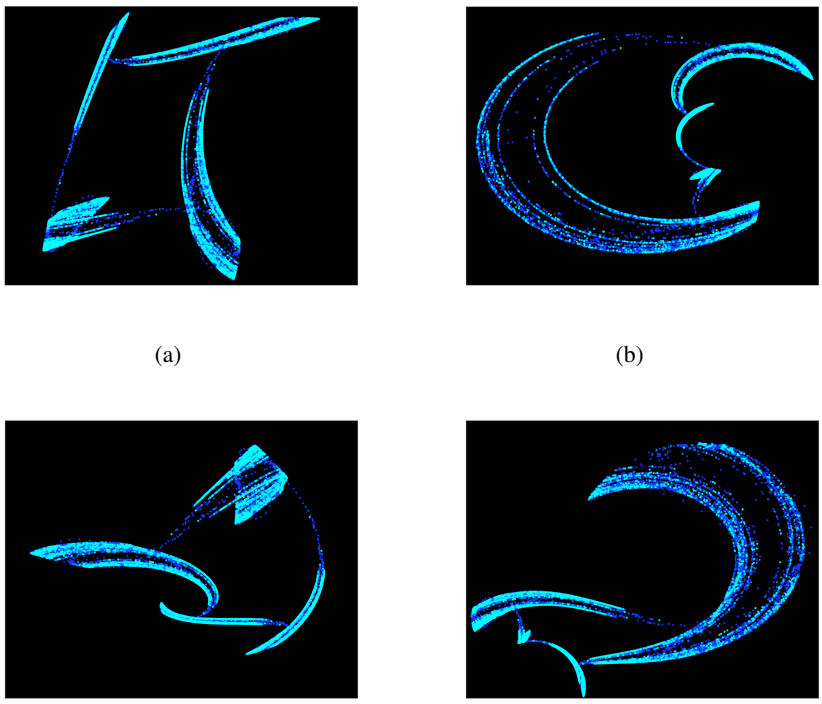

(a) (b)

(c) (d)

Figure 15. Application of non-linear transformations f_1 and f_2 to an SA; (a) Original SA (Figure 3(f)) ($\mathcal{S}$)); (b) Non-linear transformation $f_1(\mathcal{S})$; (c) Non-linear transformation $f_2(\mathcal{S})$; (d) Composition $f_1(f_2(\mathcal{S}))$.

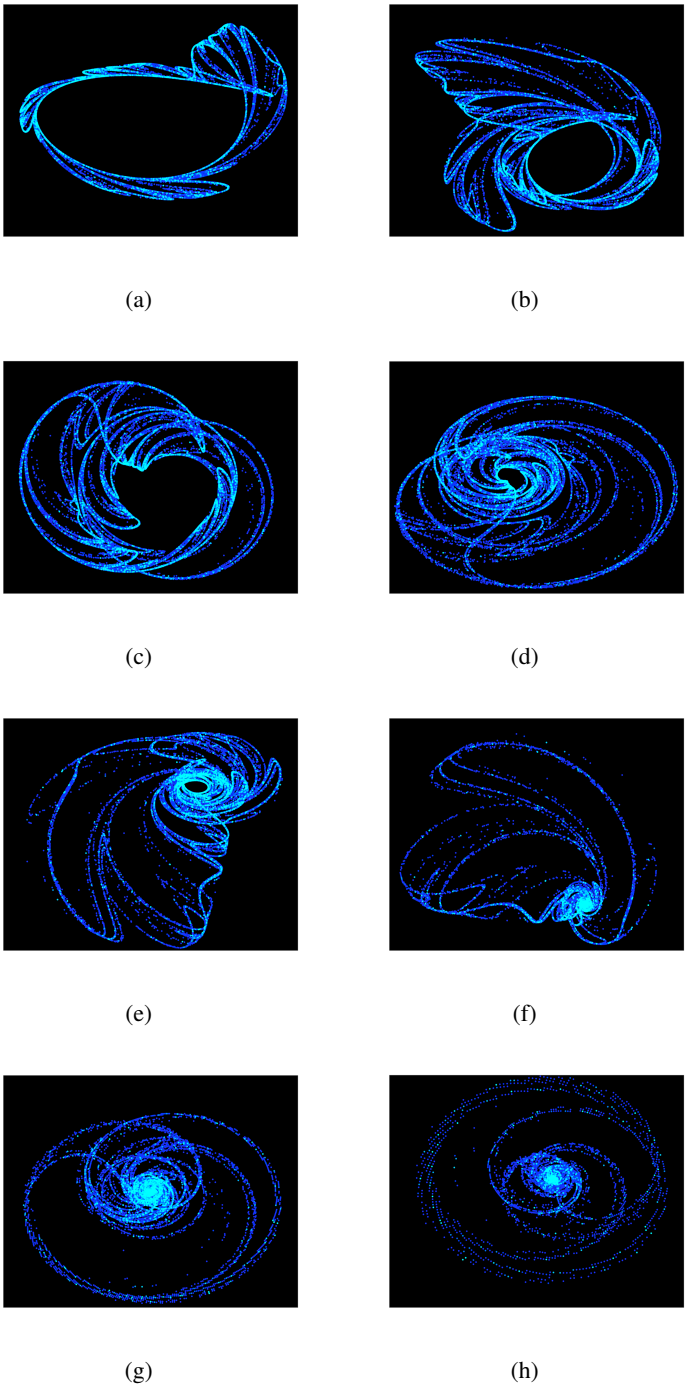

Figure 16. Recursive composition of non-linear transformations f_1 and f_2 to an SA aggregate; (a) Original SA (Figure 3(b)) ($\mathcal{S}$)); (b) $f_2(\mathcal{S})$; (c) $f_1(f_2(\mathcal{S}))$; (d) $f_2(f_1(f_2(\mathcal{S})))$; (e) $f_1(f_2(f_1(f_2(\mathcal{S}))))$; (f) $f_2(f_1(f_2(f_1(f_2(\mathcal{S})))))$; (g) $f_1(f_2(f_1(f_2(f_1(f_2(\mathcal{S}))))))$; (h) $f_2(f_1(f_2(f_1(f_2(f_1(f_2(\mathcal{S}))))))))$.

4. Conclusions

Fractal aggregates are aesthetic images usually generated in 2D real spaces using different techniques, such as non-equilibrium growth models, Iterated function systems, Lindenmayer systems or strange attractors, among others. In this paper we analyze the effect of applying combinations of non-linear transformations on known fractal structures and aggregates, to obtain new fractal images. We have selected five different known non-linear transformations and we have combined them and evaluated their capacity for forming new fractal images and aggregates from existing fractal structures. We have shown how the non-linear transformations tested may have different effects over the initial fractal structures: Some of them act by "bending" the initial aggregates, others act similarly to a "diffusion" process, and the combination of these effects forms aesthetic new fractal images with great potential as artwork. We have also shown that the aesthetic final result of the non-linear transformations combination fully depends on the original image. In the experimental section of this paper, we have discussed the effect of non-linear transformation combinations on classical fractal patterns such as the Sierpinski triangle and Sierpinski carpet, and we have also shown that some strange attractors may produce highly aesthetic artwork images after applying a combination of non-linear transformations. Further research may include studies on the effect of applying new non-linear transformations to existing fractal structures, and the application of AI-based algorithms such as neural network models or support vector machines as new potential non-linear transformation sources.

Appendix

Quadratic map parameters for strange attractors fractals construction

Table 2. Parameters of the quadratic map to generate the SAs depicted in Figure 3 (initial point $[0.6, 0.9]$).

Attractor	Quadratic map parameters (a_1-a_{12}), Eq (2.4)
(a)	$(-0.3, 0.1, 0.6, -0.7, -1.1, 1.0, 0.4, -0.9, -0.1, 0.3, 1.1, -1.0)$
(b)	$(-0.2, 0.2, 0.9, 1, -0.8, 0.1, 0.5, 0.8, -1.0, 0, -0.3, 0.3)$
(c)	$(1.1, 0.7, -0.7, 0.5, -1.2, 0.0, -0.3, 0.6, 0.3, -0.1, -0.8, 0.8)$
(d)	$(0.5, -0.1, 0, -0.8, 0.9, 0.6, -1.1, -0.3, 1.2, -0.7, 1, 0.3)$
(e)	$(1.2, 0.1, -0.2, 1.1, -0.6, -0.3, 0.5, 0.9, -1.2, 0.4, -0.5, 0.3)$
(f)	$(-0.8, 0, 0.4, -0.3, 1.1, 1.2, -1.2, -1, 0.7, -0.6, 0.5, 1)$
(g)	$(0.7, -0.5, -0.4, 0, -0.2, 1.1, 1, 0.2, -1.2, 0.5, -0.3, -0.7)$
(h)	$(0.6, 1.1, -0.1, -1.2, 0.8, 0.1, 0.3, -0.8, 0.7, 0.4, -0.3, -0.2)$
(i)	$(0.64, -0.23, 1.39, 0, -1.91, 1.52, 0.34, 1.15, 0.19, 1.96, -1.29, -0.02)$

Sierpinski carpet IFS

$$T_6 = \begin{cases} \begin{pmatrix} x_{n+1} \\ y_{n+1} \end{pmatrix} = \begin{pmatrix} 1/3 & 0 \\ 0 & 1/3 \end{pmatrix} \cdot \begin{pmatrix} x_n \\ y_n \end{pmatrix} + \begin{pmatrix} 0 \\ 0 \end{pmatrix} & p = 1/8 \\ \begin{pmatrix} x_{n+1} \\ y_{n+1} \end{pmatrix} = \begin{pmatrix} 1/3 & 0 \\ 0 & 1/3 \end{pmatrix} \cdot \begin{pmatrix} x_n \\ y_n \end{pmatrix} + \begin{pmatrix} 0 \\ 1/3 \end{pmatrix} & p = 1/8 \\ \begin{pmatrix} x_{n+1} \\ y_{n+1} \end{pmatrix} = \begin{pmatrix} 1/3 & 0 \\ 0 & 1/3 \end{pmatrix} \cdot \begin{pmatrix} x_n \\ y_n \end{pmatrix} + \begin{pmatrix} 0 \\ 2/3 \end{pmatrix} & p = 1/8 \\ \begin{pmatrix} x_{n+1} \\ y_{n+1} \end{pmatrix} = \begin{pmatrix} 1/3 & 0 \\ 0 & 1/3 \end{pmatrix} \cdot \begin{pmatrix} x_n \\ y_n \end{pmatrix} + \begin{pmatrix} 1/3 \\ 0 \end{pmatrix} & p = 1/8 \\ \begin{pmatrix} x_{n+1} \\ y_{n+1} \end{pmatrix} = \begin{pmatrix} 1/3 & 0 \\ 0 & 1/3 \end{pmatrix} \cdot \begin{pmatrix} x_n \\ y_n \end{pmatrix} + \begin{pmatrix} 1/3 \\ 2/3 \end{pmatrix} & p = 1/8 \\ \begin{pmatrix} x_{n+1} \\ y_{n+1} \end{pmatrix} = \begin{pmatrix} 1/3 & 0 \\ 0 & 1/3 \end{pmatrix} \cdot \begin{pmatrix} x_n \\ y_n \end{pmatrix} + \begin{pmatrix} 2/3 \\ 0 \end{pmatrix} & p = 1/8 \\ \begin{pmatrix} x_{n+1} \\ y_{n+1} \end{pmatrix} = \begin{pmatrix} 1/3 & 0 \\ 0 & 1/3 \end{pmatrix} \cdot \begin{pmatrix} x_n \\ y_n \end{pmatrix} + \begin{pmatrix} 2/3 \\ 1/3 \end{pmatrix} & p = 1/8 \\ \begin{pmatrix} x_{n+1} \\ y_{n+1} \end{pmatrix} = \begin{pmatrix} 1/3 & 0 \\ 0 & 1/3 \end{pmatrix} \cdot \begin{pmatrix} x_n \\ y_n \end{pmatrix} + \begin{pmatrix} 2/3 \\ 2/3 \end{pmatrix} & p = 1/8 \end{cases}$$

Author contributions

S. Salcedo-Sanz: Conceptualization, formal analysis, software, writing—original draft preparation; S. Salcedo-Sanz and J. Pérez-Aracil: Methodology; S. Salcedo-Sanz, P. Álvarez-Couso, L. Castelo-Sardina and J. Pérez-Aracil: Investigation, writing—review and editing; P. Álvarez-Couso and L. Castelo-Sardina: Supervision. All authors have read and agreed to the published version of the manuscript.

Use of Generative-AI tools declaration

The authors declare they have not used Artificial Intelligence (AI) tools in the creation of this article.

Acknowledgments

This research has been partially supported by the project PID2023-150663NB-C21 of the Spanish Ministry of Science and Innovation (MICINN).

Conflict of interest

All authors declare no conflicts of interest in this paper.

References

1. C. J. Evertsz, B. B. Mandelbrot, Fractal aggregates, and the current lines of their electrostatic potentials, *Physica A*, **177** (1991), 589–592. https://doi.org/10.1016/0378-4371(91)90205-Q
2. D. J. Aks, J. C. Sprott, Quantifying aesthetic preference for chaotic patterns, *Empir. Stud. Arts*, **14** (1996), 1–16.
3. T. A. Witten, L. M. Sander, Diffusion-limited aggregation, *Phys. Rev. B*, **27** (1983), 5686. https://doi.org/10.1103/PhysRevB.27.5686
4. P. Meakin, Formation of fractal clusters and networks by irreversible diffusion-limited aggregation, *Phys. Rev. Lett.*, **51** (1983), 1119. https://doi.org/10.1103/PhysRevLett.51.1119
5. E. Guesnet, R. Dendievel, D. Jauffrès, C. Martin, B. Yrieix, A growth model for the generation of particle aggregates with tunable fractal dimension, *Physica A*, **513** (2019), 63–73. https://doi.org/10.1016/j.physa.2018.07.061
6. J. C. Sprott, Automatic generation of iterated function systems, *Comput. Graph.*, **18** (1994), 417–425. https://doi.org/10.1016/0097-8493(94)90042-6
7. M. Barnsley, J. Hutchinson, Ö. Stenflo, A fractal valued random iteration algorithm and fractal hierarchy, *Fractals*, **13** (2005), 111–146. https://doi.org/10.1142/S0218348X05002799
8. B. Zhang, Y. Zhang, Y. Xie, Generating irregular fractals based on iterated function systems, *AIMS Math.*, **9** (2024), 13346–13357. https://doi.org/10.3934/math.2024651
9. G. Williams, Using the fractal paintbrush, *J. Math. Arts*, **3** (2009), 85–96. https://doi.org/10.1080/17513470902953396
10. L. Zhang, T. C. Chang, Y. M. Mao, *A kind of IFS fractal image generation method based on Markov random process*, In: 2019 IEEE International Conference on Computation, Communication and Engineering (ICCCE), IEEE, 2019, 1–4. https://doi.org/10.1109/ICCCE48422.2019.9010799
11. X. Tao, S. Bai, C. Liu, H. Chen, Y. Yan, *Algorithm of controllable fractal image based on ifs code*, In: 2021 IEEE International Conference on Power Electronics, Computer Applications (ICPECA), IEEE, 2021, 801–809. https://doi.org/10.1109/ICPECA51329.2021.9362569
12. M. D. Pham, Fractal approximation of chaos game representations using recurrent iterated function systems, *AIMS Math.*, **5** (2019), 1824–1840. http://dx.doi.org/10.3934/math.2019.6.1824
13. P. Grassberger, I. Procaccia, Measuring the strangeness of strange attractors, *Physica D*, **9** (1983), 189–208. https://doi.org/10.1016/0167-2789(83)90298-1
14. P. Grassberger, I. Procaccia, Characterization of strange attractors, *Phys. Rev. Lett.*, **50** (1983), 346. https://doi.org/10.1103/PhysRevLett.50.346
15. J. C. Sprott, *Strange attractors: Creating patterns in chaos*, M & T Books, New York, **9** (1993).
16. A. Lindenmayer, Mathematical models for cellular interactions in development I. Filaments with one-sided inputs, *J. Theor. Biol.*, **18** (1968), 280–299. https://doi.org/10.1016/0022-5193(68)90079-9
17. J. Mishra, S. Mishra, *L-system fractals*, Elsevier, **209** (2007).

18. P. Prusinkiewicz, J. Hanan, *Lindenmayer systems, fractals, and plants*, Springer Science & Business Media, **79** (2013). https://doi.org/10.4324/9780203111581-10

19. M. Batchelor, B. Henry, Diffusion-limited aggregation with eden growth surface kinetics, *Physica A*, **203** (1994), 566–582. https://doi.org/10.1016/0378-4371(94)90015-9

20. S. Salcedo-Sanz, L. Cuadra, Hybrid L-systems-diffusion limited aggregation schemes, *Physica A*, **514** (2019), 592–605. https://doi.org/10.1016/j.physa.2018.09.127

21. S. Salcedo-Sanz, L. Cuadra, Multi-fractal multi-resolution structures from DLA-strange attractors hybrids, *Commun. Nonlinear Sci.*, **83** (2020), 105092. https://doi.org/10.1016/j.cnsns.2019.105092

22. Z. Xia, The growth simulation of pine-needle like structure with diffusion-limited aggregation and oriented attachment, *RSC Adv.*, **12** (2022), 22946–22950. https://doi.org/10.1039/D2RA03649E

23. X. Tian, H. Xia, Crossover effects and dynamic scaling properties from Eden growth to diffusion-limited aggregation, *Phys. Lett. A*, **508** (2024), 129494. https://doi.org/10.1016/j.physleta.2024.129494

24. K. Nakamura, Iterated inversion system: An algorithm for efficiently visualizing Kleinian groups and extending the possibilities of fractal art, *J. Math. Arts*, **15** (2021), 106–136. https://doi.org/10.1080/17513472.2021.1943998

25. P. V. Loocke, Non-linear iterated function systems and the creation of fractal patterns over regular polygons, *Comput. Graph.*, **33** (2009), 698–704. https://doi.org/10.1016/j.cag.2009.05.003

26. K. Gdawiec, Star-shaped set inversion fractals, *Fractals*, **22** (2014), 1450009. https://doi.org/10.1142/S0218348X14500091

27. K. Gdawiec, Inversion fractals and iteration processes in the generation of aesthetic patterns, *Comput. Graph. Forum*, **36** (2017), 35–45. https://doi.org/10.1111/cgf.12783

28. G. Helt, Extending mandelbox fractals with shape inversions, *arXiv preprint*, 2018. https://doi.org/10.48550/arXiv.1809.01720

29. J. L. Ramirez, G. N. Rubiano, B. J. Zlobec, Generating fractal patterns by using p-circle inversion, *Fractals*, **23** (2015), 1550047. https://doi.org/10.1142/S0218348X15500474

30. P. Ouyang, K. W. Chung, A. Nicolas, K. Gdawiec, Self-similar fractal drawings inspired by mc escher's print square limit, *ACM T. Graphic.*, **40** (2021), 1–34. https://doi.org/10.1145/3447647

31. T. C. Halsey, Diffusion-limited aggregation: A model for pattern formation, *Phys. Today*, **53** (2000), 36–41. https://doi.org/10.1063/1.1333284

32. H. Stanley, A. Coniglio, S. Havlin, J. Lee, S. Schwarzer, M. Wolf, Diffusion limited aggregation: A paradigm of disorderly cluster growth, *Physica A*, **205** (1994), 254–271. https://doi.org/10.1016/0378-4371(94)90503-7

33. S. Ferreira Jr, S. Alves, A. F. Brito, J. Moreira, Morphological transition between diffusion-limited and ballistic aggregation growth patterns, *Phys. Rev. E*, **71** (2005), 051402. https://doi.org/10.1103/PhysRevE.71.051402

34. A. Ben-Mizrachi, I. Procaccia, P. Grassberger, Characterization of experimental (noisy) strange attractors, *Phys. Rev. A*, **29** (1984), 975. https://doi.org/10.1007/BF01312485

35. M. F. Barnsley, *Superfractals*, Cambridge University Press, 2006.

36. M. F. Barnsley, Transformations between self-referential sets, *Am. Math. Mon.*, **116** (2009), 291–304. https://doi.org/10.1080/00029890.2009.11920941

37. S. Salcedo-Sanz, Modern meta-heuristics based on nonlinear physics processes: A review of models and design procedures, *Phys. Rep.*, **655** (2016), 1–70. https://doi.org/10.1016/j.physrep.2016.08.001

38. P. Prusinkiewicz, *Graphical applications of L-systems*, In: Proceedings of Graphics Interface, **86** (1986), 247–253.

39. G. Irving, H. Segerman, Developing fractal curves, *J. Math. Arts*, **7** (2013), 103–121. https://doi.org/10.1080/17513472.2013.852399

40. R. F. Voss, *Random fractals: Characterization and measurement*, In: Scaling phenomena in disordered systems, Springer, 1986, 1–11.

41. A. Block, W. V. Bloh, H. Schellnhuber, Efficient box-counting determination of generalized fractal dimensions, *Phys. Rev. A*, **42** (1990), 1869. https://doi.org/10.1103/PhysRevA.42.1869

42. U. Freiberg, S. Kohl, Box dimension of fractal attractors and their numerical computation, *Commun. Nonlinear Sci.*, **95** (2021), 105615. https://doi.org/10.1016/j.cnsns.2020.105615

43. R. Wang, A. K. Singh, S. R. Kolan, E. Tsotsas, Investigation of the relationship between the 2D and 3D box-counting fractal properties and power law fractal properties of aggregates, *Fractal Fract.*, **6** (2022), 728. https://doi.org/10.3390/fractalfract6120728

AIMS Press